# Changes in a nanoparticle's spectroscopic signal mediated by the local environment



Nanotechnology **23** (2012) 485202 (6pp) doi:10.1088/0957-4484/23/48/485202

# Changes in a nanoparticle's spectroscopic signal mediated by the local environment

**R Miotto[1], F D Kiss[2,3] and A C Ferraz[2]**

[1] Centro de Ciências Naturais e Humanas, Universidade Federal do ABC, Rua Santa Adelia 166, CEP 09210-170, Santo André, SP, Brazil
[2] Instituto de Física da Universidade de São Paulo, Caixa Postal 66318, CEP 05315-970, São Paulo, SP, Brazil

E-mail: ronei.miotto@ufabc.edu.br

Received 31 August 2012, in final form 13 October 2012
Published 6 November 2012
Online at stacks.iop.org/Nano/23/485202

**Abstract**
Using a first-principles theoretical model the adsorption of a methyl radical on different sized silver nanoparticles is compared to the adsorption of the same radical on model surfaces. Calculations of our structural, dynamical and electronic properties indicated that small changes in the local environment will lead to small changes in infrared (IR) wavenumbers, but in dramatic changes in the IR signal. Our calculations indicate the lower the adsorption site coordination, the higher is the signal strength, suggesting that small changes in the electronic charge distribution will result in bigger changes in the polarizability and hence in the spectroscopic signal intensity. This effect explains, among others, the signal magnification observed for nanoparticles in surface enhanced Raman spectroscopic (SERS) experiments.

(Some figures may appear in colour only in the online journal)

## 1. Introduction

Raman spectroscopy (RS) has already proven to be a powerful technique to characterize carbon materials at a molecular level. This is because Raman spectroscopy is able to identify sample composition, chemical states of the bonds (orientation, conformation) and also provide information about intermolecular interaction [1]. Besides its ability to provide precise information at a molecular level, RS has a series of advantages: it is a non-destructive and non-invasive technique, that works *in situ* and *in vitro*, for biological samples, at a wide range of conditions [1]. However, as Raman scattering is extremely inefficient (only 1 in $10^{10}$ incident photons will undergo Raman scattering [1]), this technique was only largely explored after the observation [2] that, for certain molecules adsorbed on specially prepared metal surfaces, a Raman spectrum is observed whose intensity exceeds by a factor of $10^5$–$10^6$ what one expects on the basis of simple calculations [3]. This was then called surface enhanced Raman scattering (SERS). Generally substrates based on metals such as Ag, Au and Cu, either with roughened surfaces or in the form of nanoparticles, are required to realize a substantial SERS effect [3].

The SERS effect is thought to originate by two different mechanisms [4]: electromagnetic, with a factor of enhancement of $10^4$, and chemical, with an enhancement of the order of $10^2$. In the first case, the increase in intensity of the Raman signal occurs because of an enhancement in the electric field provided by the surface. Localized surface plamons are excited by the incident light on the surface. Scattering occurs only when the plasmon oscillations are perpendicular to the surface. Since roughened surfaces or arrangements of nanoparticles provide an area on which these localized collective oscillations can occur, they are often a choice in SERS experiments [5]. The electromagnetic theory is nicely reviewed by Moskovits in [3]. The chemical enhancement mechanism, on the other hand, does not involve surface plasmons, but a charge transfer between the chemisorbed species and the metal surface [4].

In order to explain both the electromagnetic and the chemical enhancement process, theories such as the image field model [6], the *em* model (based on the response of

[3] Present address: Universidade Federal da Integração Latino-Americana (UNILA), Avenida Tancredo Neves 6731, Parque Tecnológico de Itaipu (PTI)-Bloco 6, Espaço 1, Sala 5, CEP 85856-970, Foz do Iguaçu, PR, Brazil.

 

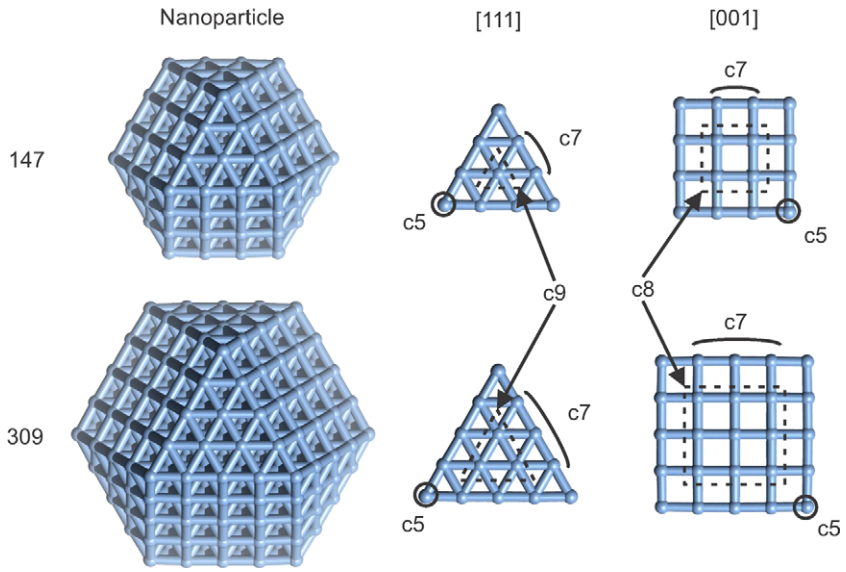


**Figure 1.** Schematic representation of nanoparticles with 147 and 309 atoms. Different adsorption sites in different surfaces are highlighted on the right-hand side. The cX symbol indicates an adsorption site with coordination X in a given area: c5, c7, c8 and c9 sites are enclosed by circles, brackets, squares and triangles, respectively.

small metal particles to electromagnetic fields) [7], or the charge transfer theory [4], were developed. The *em* model has successfully explained the major aspects of SERS, since numerical methods based on it led to a quantitative agreement between observations and calculations [8] especially for surfaces with definite patterns. As successful as the *em* theory has been, there exists a number of observations that do not seem to be properly addressed in terms of it, which include, for example, the fact that CO and $N_2$, whose Raman cross sections are almost identical, produce SERS spectra of different intensities [3]. In this sense, it is clear that although SERS is a widely used technique, there is a lack of understanding of the enhancement process at a molecular level. In order to contribute to the understanding of this issue, we have chosen a different approach: simulated vibrational spectra for the interaction of the methyl radical with various adsorption sites on silver nanoparticles are investigated using density functional theory (DFT). In this work, a systematic study correlating changes in the structural, dynamical and electronic properties of the adsorbed system and changes in the vibrational spectra peaks and intensity was carried out, with a view to provide further understanding in the signal magnification observed for nanoparticles in SERS experiments.

## 2. Theoretical modeling

Cube-octahedral nanoparticles are modeled in the supercell scheme, considering an extended bulk with a FCC crystalline packing properly cut to give the desired geometry, following the procedure described in [9], and a vacuum region greater than 10 Å. The ionic potentials are described by ultra-soft pseudopotentials [10–12] and the electron–electron exchange–correlation interactions are described within DFT considering the generalized gradient approximation as proposed by Perdew and Wang (PW91) [13]. Spin polarization effects, as considered in the Vienna *ab initio* simulation package (VASP) [14, 15], are explicitly treated. The single-particle orbitals are expressed in a plane waves base with energy up to 200 eV, considering only the Γ point inside the Brillouin zone. Increasing the number of **k**-points or the basis set results in changes in total energies, atomic distances and vibrational modes smaller than 0.1%, 0.2% and 1.0%, respectively. The atoms are assumed to be at their low energy position when the forces are smaller than 10 meV $Å^{-1}$. Vibrational loss spectra are calculated as follows: the normal modes and the corresponding frequencies are the solutions of the dynamical problem of the ions driven by the dynamical matrix, or Hessian, that is constructed with the Hellmann–Feynman forces resulting from displacements of the ions from their equilibrium positions. The intensities are derived from the dipole moment of the system calculated for each distorted geometry as proposed by Preuss *et al* [16, 17].

## 3. Results and discussion

In figure 1 nanoparticles with 147 and 309 atoms, indicated as 147 and 309 for simplicity, are shown as well as possible adsorption sites, and respective coordination numbers (cX), in the [111] and [001] surfaces. The choice of those representative nanoparticles is related to the fact that the first (147) represents the transient regime with molecular and crystal characteristics observed for nanoparticles between 1.5 and 2.0 nm, while the second (309) has a strong crystalline character, which is observed for nanoparticles larger than 2.0 nm, as discussed in [9]. The coordination sites are those found both in the nanoparticles' and on the free [111] (case of c9) and [001] (case of c8) surfaces or only in the corners of the nanoparticles (c5 and c7). Possible c5, c7, c8 and c9

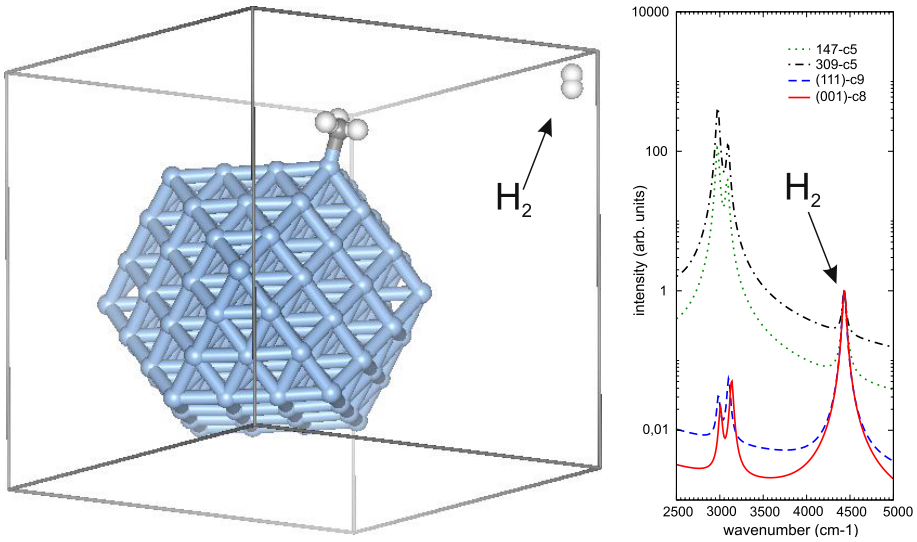


**Figure 2.** (Left) Schematic representation of the supercell indicating one adsorbed methyl radical and the $H_2$ molecule far away from the nanoparticle. Right: vibrational loss spectra for different adsorption sites, nanoparticles and ideal surfaces illustrating the use of the characteristic $H_2$ peak intensity in the normalization procedure.

**Table 1.** Adsorption energies ($E_{ads}$ in eV) and Ag–C bond length (in Å) for the adsorption sites represented in figure 1 for nanoparticles 147 and 309 and the [111] and [001] ideal surfaces.

| | c5 | | c7 | | c8 | | c9 | |
|---|---|---|---|---|---|---|---|---|
| | $E_{ads}$ | Ag–C | $E_{ads}$ | Ag–C | $E_{ads}$ | Ag–C | $E_{ads}$ | Ag–C |
| 147 | −1.43 | 2.16 | −1.38 | 2.18 | −1.12 | 2.19 | −1.32 | 2.20 |
| 309 | −1.48 | 2.15 | −1.32 | 2.17 | −1.28 | 2.19 | −1.25 | 2.20 |
| [111] | — | — | — | — | −1.03 | 2.19 | — | — |
| [001] | — | — | — | — | — | — | −1.07 | 2.20 |

sites are enclosed by circles, brackets, squares and triangles, respectively.

In table 1 we shown the adsorption energies for the considered adsorption sites in nanoparticles 147 and 309, as well as on the [111] and [001] surfaces. Our results indicate that for nanoparticles in the crystalline regime (nanoparticle 309) lower coordination adsorption sites are more energetically favorable. In a similar manner, a given adsorption site in a nanoparticle is more energetically favorable than the same site in an ideal surface. In the transient regime (nanoparticle 147), a similar picture is observed except for the c9 adsorption site.

From our theoretical data we observe that all bond lengths, namely Ag–C, Ag–Ag (not shown) and C–H (not shown) are very close, which is consistent with the experimental observation of the existence of a single vibrational loss peak in the spectra of different organic adsorbates in silver nanoparticles [3]. It is also clear from our simulations that the c5 adsorption site is the most favorable from the energy point of view for both nanoparticles 147 and 309. Therefore, in the next step of our study, we analyze the spectroscopic signal arising from the adsorption of the methyl radical in both nanoparticles.

In order to compare the intensity of different vibrational loss spectra, we have used as reference the characteristic peak of the hydrogen molecule using the following procedure: a $H_2$ molecule is included far from the nanoparticle, in order to avoid interactions between the nanoparticle and the molecule, and its vibrational modes are calculated for all considered systems. As all vibrational spectra will present the same characteristic $H_2$ loss in the same position and with the same intensity, we can use this peak in order to normalize all spectra with respect to it. This procedure is illustrated in figure 2.

In figure 3(a) we present the vibrational loss spectra obtained upon adsorption of the methyl radical on nanoparticles 147 and 309. In order to allow a better comparison, the same radical was adsorbed on the ideal [111] and [001] surfaces. As expected, it is clear in this figure that the magnitude of the signal arising from the adsorption on a nanoparticle is orders of magnitude higher than that observed for a ideal surface. However, one must bear in mind that the adsorption sites in both cases are completely different. Indeed, not only their coordination numbers are different, but also the environment of the adsorption site is clearly not the same. It is also important to mention that all vibrational loss peaks are very close to each other, which is consistent with the fact that all Ag–C and C–H bond lengths are not decisively affected by the adsorption site environment.

In order to explore the role of the environment on the magnitude of the vibrational loss signal, we have performed a systematic comparison of the adsorption on equivalent sites of the ideal surface and the considered nanoparticles.

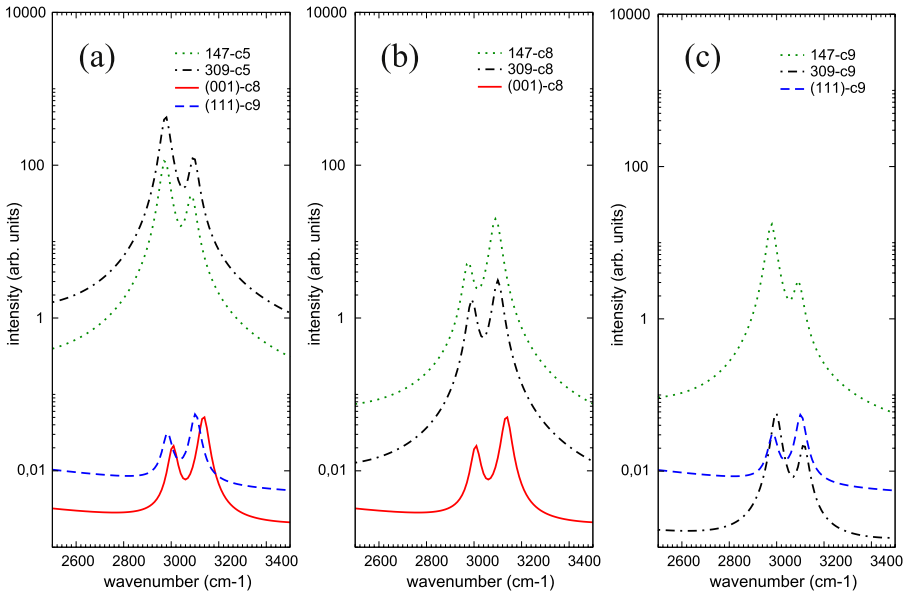


**Figure 3.** Vibrational loss spectra arising from the adsorption of the methyl radical on nanoparticles 147 and 309 and on the ideal [001] and [111] surfaces considering: (a) the most energetically favorable adsorption site (c5) in the case of nanoparticles 147 and 309, c8 for the ideal [001] and c9 for the ideal [111] surfaces; (b) c8 adsorption site in nanoparticles 147 and 309 and the ideal [001] surface; and (c) c9 adsorption site in nanoparticles 147 and 309 and the ideal [111] surface.

This is depicted in figure 3, where loss spectra obtained upon adsorption of the methyl radical on the c8 and c9 site of the nanoparticles are compared to the signal arising from the adsorption on the same site of the ideal [111] or [001] surface. For the c8 site, our results indicate an amplification of the signal for both nanoparticles 147 and 309, but with a magnitude smaller than that observed for the most favorable adsorption site (c5). It is also interesting to note that, in this case, the vibrational loss amplification is smaller for nanoparticle 309. For the c9 adsorption site, on the other hand, the signal amplification is only clearly seen for nanoparticle 147. Our results can be directly correlated with the systems environment in each case if we consider the circular, square and triangular regions defining the adsorption sites in figure 1. First it is important to realize that while all c5 sites are equivalent, this symmetry is not present for the other adsorption sites. The c8 site, for example, has two c7 and two c8 neighbors when nanoparticle 147 is considered, but can have either two c7 and two c8 or four c8 neighbors (the central atom) when nanoparticle 309 is considered. If second-neighbor atoms are considered, c8 atoms can be reclassified in three different environments, as shown in figure 4. In addition, it can be clearly seen in figure 4 that when different environments are considered, non-equivalent adsorption sites will lead to slightly different vibrational loss spectra. A similar correlation between coordination of adsorption site environments and fingerprints on voltammetric profiles in Pt nanoparticles for [110], [111] and [001] facets was recently suggested by Chen *et al* [18].

In figure 3 the vibrational loss spectra shown considers the adsorption of the methyl radical on a c8 site with four c8 neighbors. Following this picture, the c8 adsorption site of nanoparticle 147 has a higher intensity since its neighbors (two c7 and two c8 atoms) represent a more heterogeneous

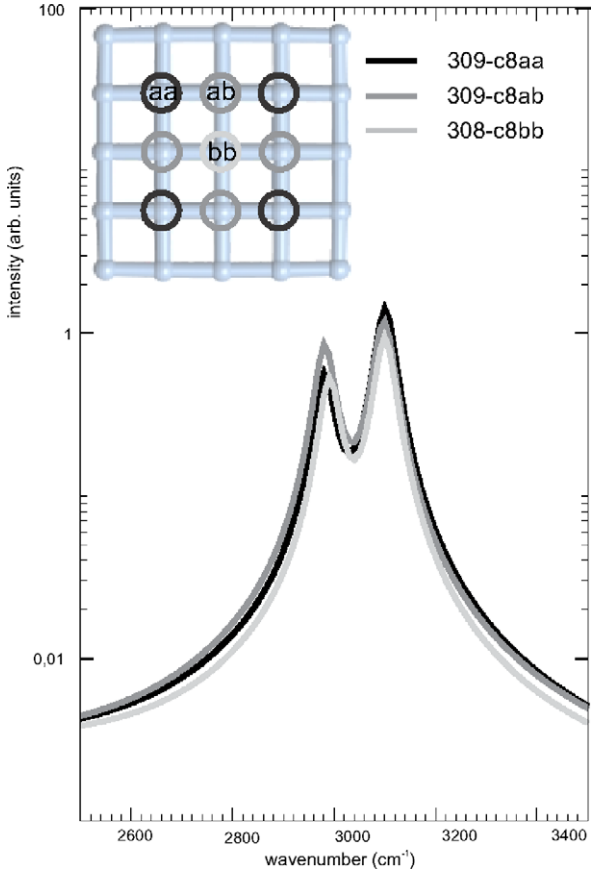


**Figure 4.** Vibrational loss spectra for the adsorption of the methyl radical on non-equivalent c8 adsorption sites, indicated in the inset by different circles, of nanoparticle 309.

environment when compared to the c8 adsorption site of nanoparticle 309 (four c8 atoms). The c9 adsorption site of nanoparticle 147, on the other hand, has only c7 neighbors,

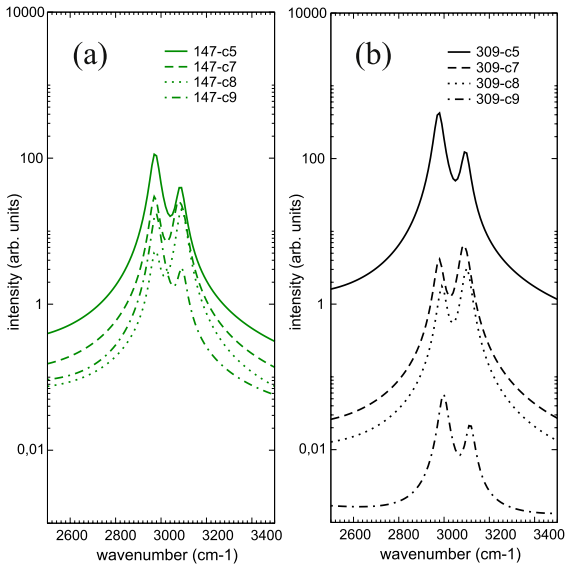


**Figure 5.** Vibrational loss spectra for the adsorption of the methyl radical on different adsorption sites in nanoparticles 147 and 309.

**Table 2.** Mean changes (in %) in the bond lengths between Ag atoms in the surface (surf.), with sub-surface Ag atoms (core) and with all neighboring atoms (total) upon adsorption of the methyl radical in the different adsorption sites represented in figure 1 for nanoparticles 147 and 309 and the [111] and [001] ideal surfaces.

| | | 147 | 309 | [111] | [001] |
|---|---|---|---|---|---|
| c5 | Surf. | 2.1 | 1.2 | — | — |
| | Core | 2.9 | 1.4 | — | — |
| | Total | 2.3 | 1.3 | — | — |
| c7 | Surf. | 1.7 | 1.4 | — | — |
| | Core | 4.0 | 2.1 | — | — |
| | Total | 2.4 | 1.6 | — | — |
| c8 | Surf. | 1.2 | 0.3 | — | 1.1 |
| | Core | 4.3 | 4.3 | — | 3.1 |
| | Total | 2.8 | 2.3 | — | 2.1 |
| c9 | Surf. | 1.0 | 1.0 | 0.9 | — |
| | Core | 5.4 | 4.5 | 4.0 | — |
| | Total | 2.5 | 2.5 | 1.9 | — |

while in nanoparticle 309 there are four c7 and two c9 sites. In this latter case, as c9 sites are the ideal surface sites, the spectroscopic signal is closer to that observed for the ideal surface. The small variations in the intensity and position of the peaks are probably due to perturbations related to the neighboring c7 sites. Increasing the size of the nanoparticle will not dramatically change this picture, since non-equivalent c8 and c9 sites will be observed. This is a clear indication that the size of the nanoparticle cannot be considered alone as the origin of the amplification of the vibrational loss signal. Indeed, Glaspell *et al* [19] have already suggested that the initial spectra show a particle size dependent enhancement. Their data indicated that there is a critical size, 11 nm in the case of silver nanoparticles, for signal enhancement. However, while their experimental results only explored the size aspect, our theoretical simulations clearly indicate that the surface environment plays a significant role in this process.

Figure 5 presents the vibrational loss spectra for the adsorption of the methyl radical on different adsorption sites in nanoparticles 147 and 309 . For both nanoparticles (147 and 309), there is a clear amplification of the vibrational loss signal with the reduction of the coordination number of the adsorption site (c9 → c8 → c7 → c5). This amplification is more pronounced for nanoparticle 309 and can be explained in terms of the number of first c9 neighbors. For nanoparticle 309, for example, the c9 adsorption site has two c9 neighbors, the c8 site has only c8 neighbors, the c7 has c7, c8 and c9 neighbors and the c5 adsorption site has only c7 neighbors. Following this analysis, we understand that the smaller the number of c9 neighboring sites (or alternatively neighboring sites with higher coordination number) the higher is the amplification of the vibrational loss signal. In other words, the closer the environment is to the ideal surface, characterized by c9 sites, the smaller is the loss signal amplification.

In order to further explore the extent of the role of the environment in the properties of the system, we explore changes in the bond lengths after the interaction of the methyl radical with different silver adsorption sites. As indicated in table 2, upon adsorption the Ag–Ag bond lengths only experience a small contraction. On average this contraction is very close to that observed for the ideal surfaces (∼2.0%). The deviations, when compared to the ideal surfaces, are higher (of the order of 1%) when only the bonds between the adsorption site with sub-surface atoms are considered, indicating a smaller expansion for small coordinated adsorption sites: c5(2.9) → c7(4.0) → c8(4.3) → c9(5.4) for nanoparticle 147 and c5(1.4) → c7(2.1) → c8(4.3) → c9(5.5) for nanoparticle 309. The surface–surface bond changes, on the other hand, present no clear pattern. Indeed, from our results it was not possible to find a clear relation between changes in the local atomic structure and changes in the vibrational loss signal intensity.

In a similar manner, our simulation also indicates that there are no clear changes in the electronic charge distribution upon adsorption of the methyl radical in different adsorption sites of different nanoparticles or ideal surfaces, as illustrated in figure 6. Indeed, even when a local minimum where a small change in the Ag–C bond angle is observed is considered, as is the case of nanoparticle 309 depicted in figure 6(d), no clear changes in the electronic charge distribution are seen. As the vibrational loss signal intensity is directly related to the system's polarizability and the latter is influenced by the system's charge distribution, it is clear that small changes in charge distribution are responsible for the changes in the signal intensity. We believe that the absence of clear bonds between changes in the atomic and electronic properties of the system and changes in the vibrational loss spectra signal further supports our indication that the physical origin of the SERS effect can be directly correlated with changes in the local environment. In other words, our data suggest that small differences in the vicinities of the adsorption sites can lead to noticeable changes in the spectroscopic signal intensity.

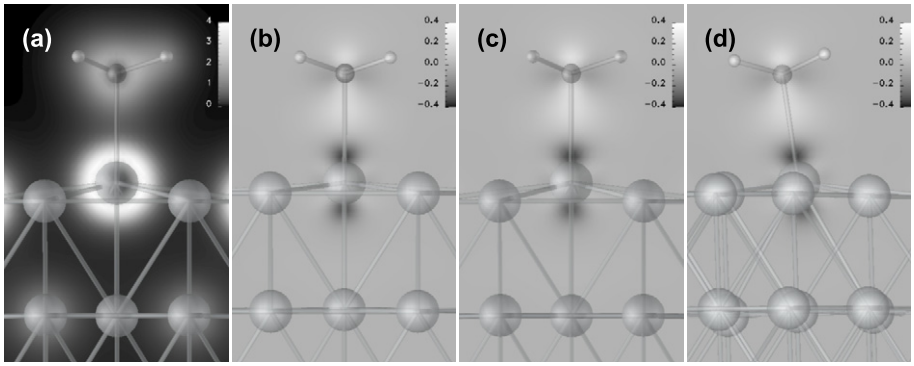


**Figure 6.** (a) Total charge density contour plot for the adsorption of the methyl radical on the c9 adsorption site of nanoparticle 147. Charge transfer (charge loss and charge gain upon adsorption) density contour plots for the adsorption of the methyl radical on the c9 adsorption site of the ideal [111] surface (b), nanoparticle 147 (c), and nanoparticle 309 (d). In the case of nanoparticle 309, only a small change in the Ag–C bond angle is observed. However, as indicated in the text, all other atomic, electronic and dynamical properties are similar to those observed for other systems.

## 4. Conclusions

In summary, from a first-principles calculations, it was possible to show that no clear correlation can be made between the atomic and electronic properties of the system and changes in the vibrational loss spectra signal. Small changes in the local environment, on the other hand, will lead to small changes in infrared (IR) wavenumbers, but in dramatic changes in the IR signal. Our calculations indicate a direct correlation between the adsorption site coordination and changes in the vibrational loss spectra signal: the smaller the coordination, the higher the signal. From the microscopic point of view, our simulations indicate that small changes in the electronic charge distribution will result in bigger changes in the polarizability and hence in the spectroscopic signal intensities. This effect explains, among other things, the signal magnification observed for nanoparticles in surface enhanced Raman spectroscopic (SERS) experiments.

## Acknowledgments

The authors acknowledge financial support from CNPq and FAPESP. This work was partially developed at the LCCA-USP computational facilities.

## References

[1] McCreery R L 2000 *Raman Spectroscopy for Chemical Analysis* (New York: Wiley) ISBN: 0471252875
[2] Fleischmann M, Hendra P J and McQuillan A J 1974 *Chem. Phys. Lett.* **26** 163–6
[3] Moskovits M 1985 *Rev. Mod. Phys.* **57** 783–826
[4] Lombardi J R, Birke R L, Lu T and Xu J 1986 *J. Chem. Phys.* **84** 4174–80
[5] Smith E and Dent G 2005 *Modern Raman Spectroscopy: A Practical Approach* (New York: Wiley) ISBN: 9780471497943
[6] King F W, Duyne R P V and Schatz G C 1978 *J. Chem. Phys.* **69** 4472–82
[7] Kerker M, Wang D S and Chew H 1980 *Appl. Opt.* **19** 4159–74
[8] Stiles P L, Dieringer J A, Shah N C and Duyne R P V 2008 *Annu. Rev. Anal. Chem.* **1** 601–26
[9] Kiss F D, Miotto R and Ferraz A C 2011 *Nanotechnology* **22** 275708
[10] Vanderbilt D 1985 *Phys. Rev.* B **32** 8412–5
[11] Vanderbilt D 1990 *Phys. Rev.* B **41** 7892–5
[12] Kresse G and Joubert D 1999 *Phys. Rev.* B **59** 1758–75
[13] Perdew J P, Chevary J A, Vosko S H, Jackson K A, Pederson M R, Singh D J and Fiolhais C 1992 *Phys. Rev.* B **46** 6671–87
[14] Kresse G and Furthmüller J 1996 *Phys. Rev.* B **54** 11169–86
[15] Kresse G and Furthmüller J 1996 *Comput. Mater. Sci.* **6** 15
[16] Preuss M and Bechstedt F 2006 *Phys. Rev.* B **73** 155413
[17] Preuss M, Miotto R, Bechstedt F, Rada T, Richardson N V and Schmidt W G 2006 *Phys. Rev.* B **74** 115402
[18] Chen Q S, Vidal-Iglesias F J, Solla-Gullon J, Sun S G and Feliu J M 2012 *Chem. Sci.* **3** 136–47
[19] Glaspell G P, Zuo C and Jagodzinski P W 2005 *J. Cluster Sci.* **16** 39–51